Turkish J. Eng. Env. Sci.
28 (2004) , 381 – 395.
© TÜBİTAK

A Parametric Analysis of Rotating Variable Thickness Elastoplastic Annular Disks Subjected to Pressurized and Radially Constrained Boundary Conditions

Ahmet N. ERASLAN, Yusuf ORÇAN
Middle East Technical University, Department of Engineering Sciences,
Ankara-TURKEY
e-mail: aeraslan@metu.edu.tr

Received 19.07.2004

Abstract

This article presents a comprehensive parametric analysis of rotating variable thickness elastoplastic annular disks with inner boundaries subject to pressure or mounted on rigid inclusion. A computer model based on von Mises yield criterion, J_2- deformation theory and nonlinear isotropic hardening is developed. Elastic limit angular velocities, partially plastic deformations and plastic limit angular velocities are investigated with emphasis on the determination of the effects of all the geometric, material and hardening parameters involved.

Key words: Stress analysis, Elastoplasticity, Variable thickness, Von Mises criterion, Nonlinear strain hardening.

Introduction

The accurate determination of stresses in rotating disks is important for an efficient design and material usage in engineering applications such as rotors of rotating machinery, flywheels and shrink fits. Therefore much research has been conducted in this field.

Until recently, closed form solutions of the problem were limited to uniform disk thicknesses (Gamer, 1984). Güven (1992) and Eraslan and Orçan (2002a, 2002b) derived the closed form solutions of variable thickness rotating disks using Tresca's yield condition and its associated flow rule. Approximate analytical (Yeh and Han, 1994; You and Zhang, 1999) and numerical solutions using perturbation (You *et al.*, 1997) or finite elements (You *et al.*, 2000; Ma *et al.*, 2001) have also been reported.

In his articles related to the present study, Güven obtained an analytical solution of the problem of rotating variable thickness disks with rigid inclusion for the elastic-plastic (Güven, 1998) and fully plastic state (Güven, 1997). His analyses were based on Tresca's yield criterion, its associated flow rule and linear strain hardening material. It was found that the plastic core of the hyperbolic annular disk consisted of 3 parts with different forms of Tresca's yield criterion in the elastic-plastic as well as in the fully plastic states.

The solution of elastic-plastic problems of rotational symmetry using Tresca's yield criterion needs separate treatment in each region due to different forms of the yield criterion in different parts of the plastic zone. In particular, in the case when a plastic region expands over a plastically predeformed region the task becomes quite cumbersome. On the other hand, one has to carry out a single formulation for the whole plastic region in the case of the von Mises yield criterion. However, this analysis is essentially numerical due to the nonlinearity involved in the use of the von Mises yield criterion. Moreover, the treatment of different boundary conditions may cause additional difficulties in the analysis.

Elastic limit angular velocities of variable thick-

ness rotating disks in power function form mounted on rigid shafts were investigated by Eraslan and Argeso (2002). Using the von Mises yield criterion and deformation theory of plasticity, plastic limit angular velocities were also estimated for linear and nonlinear hardening material behavior. A detailed analysis of inelastic behavior of constant and variable thickness rotating annular disks with rigid inclusion using the von Mises yield criterion was presented by Eraslan (2002). The stresses and deformations were studied for thickness variations in power and exponential forms. Neither of these studies covers the elastic-partially plastic deformation of variable thickness annular disks. They concentrate only on the elastic limit and fully plastic limit angular velocities and the corresponding stress states.

The aim of the present work is to perform a comprehensive parametric analysis of elastic-plastic deformation of variable thickness annular disks subjected to 2 different boundary conditions on the inner boundaries that are encountered frequently in engineering applications: (i) pressurized inner and free outer boundaries, and (ii) radially constrained inner and free outer boundaries. The von Mises yield criterion and J_2- deformation theory of plasticity are employed.

It is assumed that the annular disk of inner radius a and outer radius b is symmetric with respect to the mid plane and the variability of the thickness is in the radial direction according to the form

$$h(r) = h_0\left[1 - n\,\left(\frac{r}{b}\right)^k\right] \tag{1}$$

where h_0 is the thickness at the axis, and n and k are the geometric parameters. The disk geometries for convex ($n = 0.4$, $k = 2.4$) and concave ($n = 0.4$, $k = 0.7$) profiles are shown in Figure 1.

The Analysis

For a state of plane stress ($\sigma_z = 0$) and with the assumption of small deformations, the strain-displacement relations $\varepsilon_r = du/dr$ and $\varepsilon_\theta = u/r$, the equation of motion in radial direction

$$\frac{d}{dr}\left(hr\sigma_r\right) - h\sigma_\theta = -h\rho\omega^2 r^2 \tag{2}$$

the compatibility relation

$$\frac{d}{dr}\left(r\varepsilon_\theta\right) - \varepsilon_r = 0 \tag{3}$$

and generalized Hooke's law

$$\varepsilon_r = \varepsilon_r^p + \frac{1}{E}[\sigma_r - \nu\sigma_\theta] \tag{4}$$

$$\varepsilon_\theta = \varepsilon_\theta^p + \frac{1}{E}[\sigma_\theta - \nu\sigma_r] \tag{5}$$

are valid irrespective of the material behavior. In the equations above σ_r and σ_θ denote the radial and circumferential stress components, ρ the density of the material, ω the angular velocity, ε_r and ε_θ the radial and circumferential strain components, E the modulus of elasticity and ν the Poisson's ratio. The superscript p indicates the plastic component.

Defining the stress function in terms of radial stress

$$Y(r) = rh\sigma_r \tag{6}$$

and using the equation of motion (2) one obtains

$$\sigma_r = \frac{Y}{hr} \text{ and } \sigma_\theta = \rho\omega^2 r^2 + \frac{1}{h}\frac{dY}{dr} \tag{7}$$

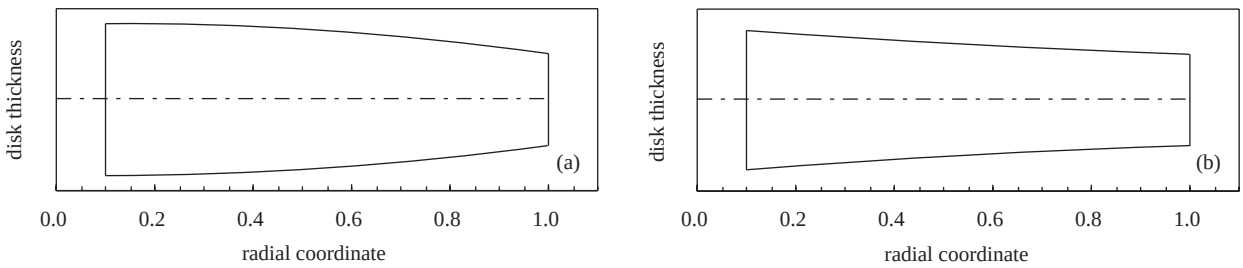

Figure 1. Variable (a) convex ($n = 0.4$, $k = 2.4$) and (b) concave ($n = 0.4$, k=0.7) disk profiles.

Expressing the elastic strains in terms of the stress function $Y(r)$ and substituting them in the compatibility relation lead to

$$\frac{d^2Y}{dr^2}+\left[\frac{1}{r}-\frac{h'}{h}\right]\frac{dY}{dr}-\left[\frac{1}{r^2}-\frac{\nu\,h'}{rh}\right]Y= -(3+\nu)\,h\rho\omega^2 r \tag{8}$$

which is the governing differential equation for the elastic region. In Eq. (8) a prime stands for differentiation with respect to radial coordinate r. On the other hand, for plane stress, the von Mises yield condition reads

$$\sigma_y=\sqrt{\sigma_r^2-\sigma_r\sigma_\theta+\sigma_\theta^2} \tag{9}$$

Using Swift's hardening law, the relation between the yield stress σ_y and the equivalent plastic strain ε_{EQ} can be expressed as

$$\sigma_y=\sigma_0\left(1+\eta\,\varepsilon_{EQ}\right)^{1/m} \tag{10}$$

where σ_0 is the yield limit, η the hardening parameter and m the material parameter. For $m=1$ linear strain hardening is obtained. The inverse relation is

$$\varepsilon_{EQ}=\left[\left(\frac{\sigma_y}{\sigma_0}\right)^m-1\right]\frac{1}{\eta} \tag{11}$$

The use of a polynomial relationship in expressing the yield stress equivalent plastic strain relation instead of (10) is discussed in You *et al.* (2000). According to J_2-deformation theory, the plastic strains are given by (Chackrabarty, 1987; Chen and Han, 1988)

$$\varepsilon_r^p=\frac{\varepsilon_{EQ}}{\sigma_y}\left[\sigma_r-\frac{1}{2}\sigma_\theta\right] \tag{12}$$

$$\varepsilon_\theta^p=\frac{\varepsilon_{EQ}}{\sigma_y}\left[\sigma_\theta-\frac{1}{2}\sigma_r\right] \tag{13}$$

$$\varepsilon_z^p=-\left(\varepsilon_r^p+\varepsilon_\theta^p\right) \tag{14}$$

Here it should be noted that the above expressions for the plastic strains are exact for proportional loading, i.e. when the ratio of deviatoric stress components is held constant. However, several authors (Chen, 1973; Jahed *et al.*, 1998) have pointed out the applicability of total deformation theory, and Budiansky (1959) showed that the total deformation theory of plasticity may be used for a range of loading paths other than proportional loading without violating the general requirements for physical soundness of a plasticity theory. Furthermore, since the objective of the present work is to perform a parametric analysis (i.e. to find out the relative effect of different parameters) the deformation theory of plasticity is adopted because of its convenience.

Substituting the total strains from Eqs. (4) and (5) in the compatibility relation (3) leads to the governing differential equation for the plastic region

$$(1+\nu)\;(\sigma_r-\sigma_\theta)+r\left[\nu\frac{d\sigma_r}{dr}-\frac{d\sigma_\theta}{dr}\right]= E\left[\varepsilon_\theta^p+r\frac{d\varepsilon_\theta^p}{dr}-\varepsilon_r^p\right] \tag{15}$$

which takes the following form in terms of the stress function $Y(r)$

$$\frac{d^2Y}{dr^2}+\left[\frac{1}{r}-\frac{h'}{h}\right]\frac{dY}{dr}-\left[\frac{1}{r^2}-\frac{\nu\,h'}{rh}\right]Y= -(3+\nu)\,h\rho\omega^2 r-\frac{Eh}{r}\left[\varepsilon_\theta^p+r\frac{d\varepsilon_\theta^p}{dr}-\varepsilon_r^p\right] \tag{16}$$

For the numerical solution of Eq. (16) a nonlinear shooting-method using a Newton-Raphson scheme with a numerically approximated tangent is designed. For this purpose, first the plastic strains on the right are expressed in terms of the stress function $Y(r)$ by noting that

$$\frac{d\varepsilon_\theta^p}{dr}=\frac{\sigma_y\left(\sigma_r'-2\sigma_\theta'\right)-\sigma_y'\left(\sigma_r-2\sigma_\theta\right)}{2\eta\sigma_y^2}- \frac{1}{2\eta\sigma_y^2}\left(\frac{\sigma_y}{\sigma_0}\right)^m\left[\begin{array}{l}(m-1)\,\sigma_y'\left(\sigma_r-2\sigma_\theta\right)+\\ \sigma_y\left(\sigma_r'-2\sigma_\theta'\right)\end{array}\right] \tag{17}$$

in which

$$\sigma_y'=\frac{\sigma_r}{\sigma_y}\left(\sigma_r'-\frac{1}{2}\sigma_\theta'\right)+\frac{\sigma_\theta}{\sigma_y}\left(\sigma_\theta'-\frac{1}{2}\sigma_r'\right) \tag{18}$$

$$\sigma_r=\frac{Y}{hr}\;\text{ and }\;\sigma_r'=-\left[\frac{1}{hr^2}+\frac{h'}{h^2r}\right]Y+\frac{Y'}{hr} \tag{19}$$

$$\sigma_\theta = \rho\omega^2 r^2 + \frac{1}{h}\frac{dY}{dr} \text{ and } \sigma'_\theta = \rho\omega^2 r - \frac{h'Y'}{h^2} + \frac{Y''}{h} \tag{20}$$

Collecting the coefficients of Y, Y' and Y'', Eq. (16) is then cast into the general form

$$\frac{d^2Y}{dr^2} = f(r, Y, \frac{dY}{dr}) \tag{21}$$

Letting $\phi_1 = Y$ and $\phi_2 = Y'$, Eq. (21) is converted into a system of initial value problems (IVP)

$$\frac{d\phi_1}{dr} = \phi_2 \tag{22}$$

$$\frac{d\phi_2}{dr} = f(r, \phi_1, \phi_2) \tag{23}$$

subject to the initial conditions

$$\phi_1^0 = Y(r = a) \text{ and } \phi_2^0 = Y'(r = a) \tag{24}$$

In the case of an annular disk subject to internal pressure p, from Eq. (6) $\phi_1^0 = -ah(a)p$ but ϕ_2^0 is not known. Since $\sigma_r(b) = 0$ implies $Y(b) = 0$, an iterative scheme can be constructed to find out ϕ_2^0 by requiring that $Y(b) = 0$. For a strain hardening material $\sigma_y \geq \sigma_0$ in the plastic region. An elastic-plastic border r_{ep} is determined from $\sigma_y(r_{ep}) = \sigma_0$. In the adjacent elastic region, Eq. (8) is solved by imposing the continuity of ϕ_1 and ϕ_2 at r_{ep} to assure the continuity of the stresses.

Iterations begin with the initial estimate ϕ_2^0 (0) and at the k-th iteration cycle the IVP system is solved 3 times with

I. $\phi_2(0) = \phi_2^k(0)$ to give $F_1 = \phi_1(b)$

II. $\phi_2(0) = \phi_2^k(0) + \Delta\phi$ to give $F_2 = \phi_1(b)$

III. $\phi_2(0) = \phi_2^k(0) - \Delta\phi$ to give $F_3 = \phi_1(b)$

in which $\Delta\phi$ is a small increment. A better approximation for $\phi_2(0)$ can now be obtained from

$$\phi_2^{k+1}(0) = \phi_2^k(0) - \frac{(2\Delta\phi)\, F_1}{F_2 - F_3} \tag{25}$$

Iterations are repeated until $\left|\phi_2^{k+1}(0) - \phi_2^k(0)\right| < \varepsilon_T$ where ε_T represents the specified error tolerance. For an annular disk with boundary conditions $u(a) = 0$ and $\sigma_r(b) = 0$, both initial conditions ϕ_1^0 and ϕ_2^0 are unknown. The condition $u(a) = 0$ provides a relation (which is nonlinear if the region is plastic) between ϕ_1^0 and ϕ_2^0. One of them is estimated, the other one is calculated accordingly and both are corrected iteratively by imposing $Y(b) = 0$. The computational details of this procedure can be found in Eraslan (2002). The initial value system defined by Eqs. (22) and (23) for the solution of Eq. (16) is not convenient for a Runge-Kutta solution since the system may be stiff at early stages of integration. The robust stiff ODE solver LSODE by Hindmarsh (Hindmarsh, 1983), which implements Gear's stiffly stable method, is used to overcome the stiffness problem.

Numerical Results

The results are presented in terms of the following dimensionless and normalized variables: radial coordinate $\bar{r} = r/b$, bore radius $\bar{a} = a/b$, angular velocity $\Omega = \omega b\sqrt{\rho/\sigma_0}$, stress $\bar{\sigma}_j = \sigma_j/\sigma_0$, displacement $\bar{u} = uE/b\sigma_0$ strain $\bar{\varepsilon}_j = \varepsilon_j E/\sigma_0$, pressure $\bar{p} = p/\sigma_0$ and hardening parameter $H = \eta\sigma_0/E$. The distribution of stresses and radial displacement at the elastic limit angular velocity $\Omega_e = 0.8852$ for an internally pressurized annular disk ($\bar{p} = 0.25$) with geometric parameters $n = 0.4$, $k = 2.4$ and $\bar{a} = 0.2$ is shown in Figure 2. The radial stress is tensile in a majority of the disk except in the neighborhood of the bore. The stress function ϕ in Figure 2 is obtained from

$$\phi = \frac{1}{\sigma_0}\sqrt{\sigma_r^2 - \sigma_r\sigma_\theta + \sigma_\theta^2} \tag{26}$$

which corresponds to the yield stress $\bar{\sigma}_y$ in the plastic core. Note that $\phi = 1$ at the plastic-elastic border and $\phi < 1$ in the elastic region. Figures 3(a) and (b) show the effect of the parameter n on the radial and circumferential stress distribution, respectively, at the elastic limit angular velocity $\Omega_e = 0.8352$ for $n = 0$. Both stress components increase with decreasing n values and they are maximum for $n = 0$ corresponding to the uniform thickness disk.

The effect of the geometric parameter k on the elastic limit angular velocity as a function of the parameter n is depicted in Figure 4. For disk profiles with $k = 2.4$ (i.e. for larger k values) higher limit angular velocities are obtained provided that n is less than a critical value. Note that for $n = 0$ both cases

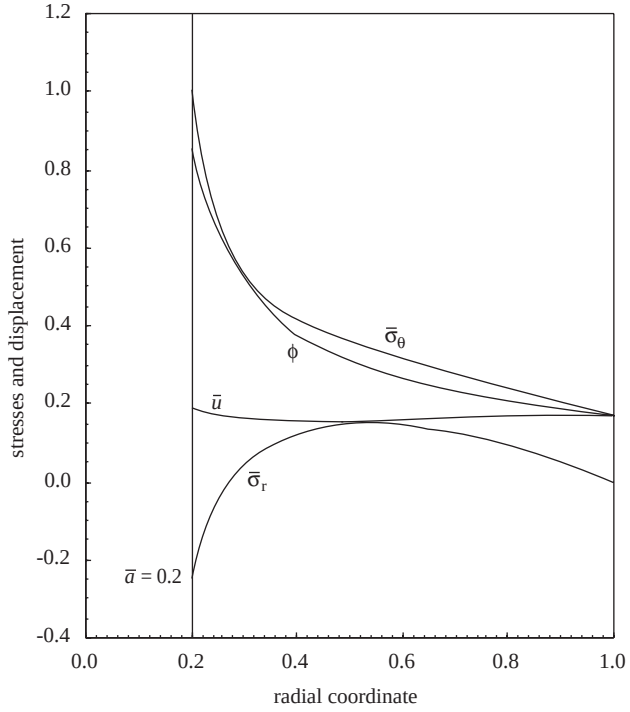

Figure 2. Stresses and displacement in a pressurized rotating annular disk for $\bar{a} = 0.2$, $n = 0.4$, $k = 2.4$ and $\bar{p} = 0.25$ at the elastic limit angular velocity $\Omega_e = 0.8352$.

reduce to a uniform thickness disk irrespective of the value of k. Figure 5 shows that elastic limit angular velocity increases with decreasing inner radius a for a fixed value of n and with increasing values of n for a fixed a. Comparing Figures 6(a) and (b) it is observed that for $m = 1$, which corresponds to linear strain hardening material, the plastic region propagates slightly further than that for $m = 0.5$, and stress and displacement distributions are almost the same, whereas the plastic strains are considerably larger. For $m = 2$ (Figure 6(c)) the circumferential stress in the plastic region decreases. The stress distribution in partially plastic annular disks for different n values is plotted in Figure 7 together with corresponding plastic strains. The angular velocity is taken to be $\Omega_{fp} = 1.8635$, which is the fully plastic limit for a constant thickness disk. Figure 8 shows that in the fully plastic state the magnitudes of σ_θ as well as σ_r are reduced by as much as 50% for $m = 2$ compared with those for $m = 0.5$. Taking $\bar{a} = 0.2$ and $m = 1$, the propagation of the elastic-plastic border $\bar{r}_{ep}$ with increasing angular velocity is calculated and plotted in Figure 9 for different hardening parameters. In Figure 10, this effect is investigated for $H = 0.4$ and different values of the parameter m. Taking $H = 0.5$, $m = 1$, $k = 1$, and $\bar{p} = 0.25$, it

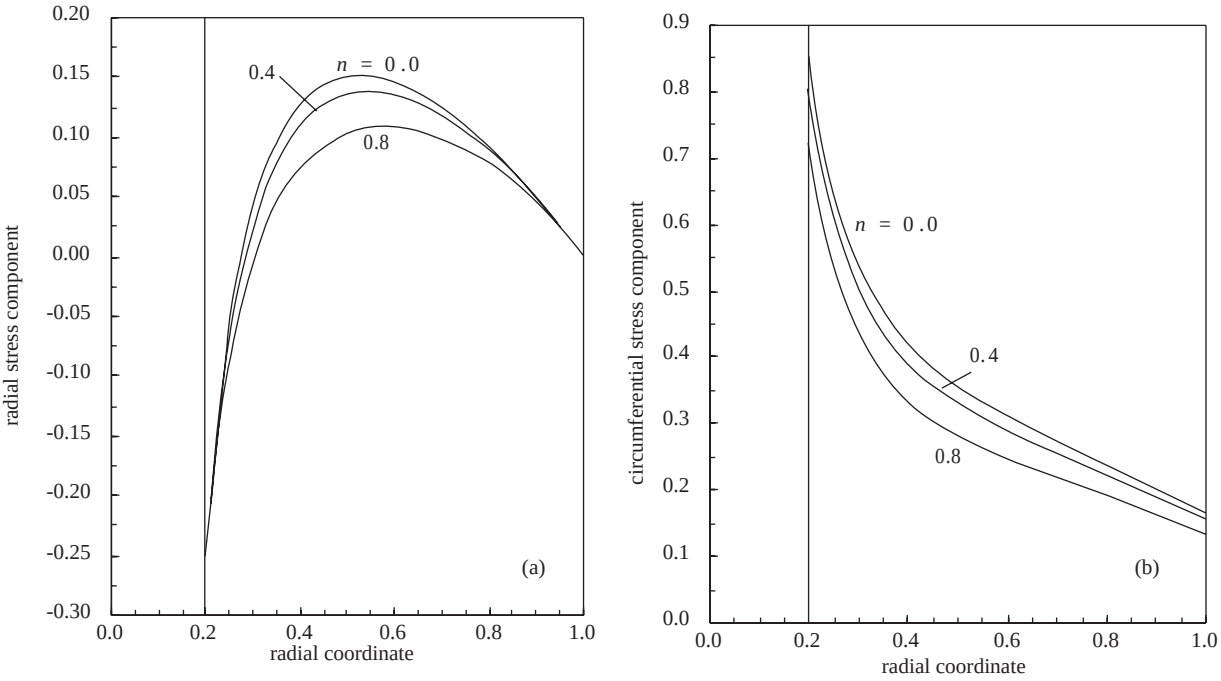

Figure 3. Comparison of (a) radial, (b) circumferential stresses for $k = 0.8$, $\Omega = 0.8352$ using n as a parameter.

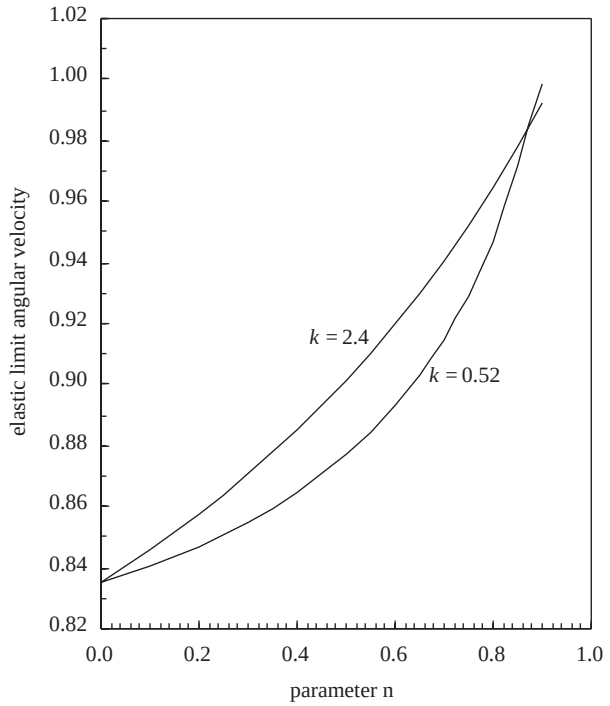

Figure 4. Variation of elastic limit angular velocity with the thickness reduction parameter n for $k = 0.52$ and $k = 2.4$.

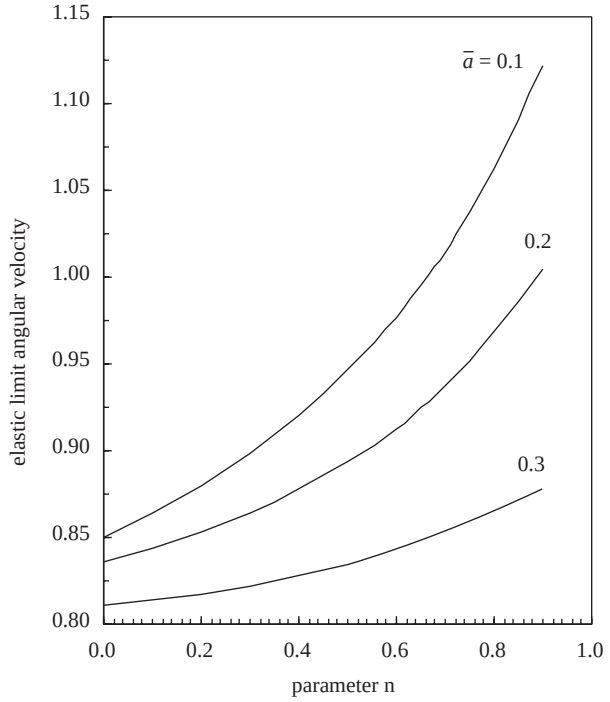

Figure 5. Variation of elastic limit angular velocity with the thickness reduction parameter n for different bore radii.

is observed in Figure 11 that the plastic limit angular velocity has a stronger dependence on a compared with the elastic limit angular velocity presented in Figure 5. Taking $\bar{a} = 0.2$, Figure 12 shows that the plastic limit angular velocity increases with increasing hardening parameter$H$ and decreasing values of m.

When an annular disk is mounted on a rigid shaft, owing to the centrifugal forces developed by rotation the stress distribution is tensile throughout the disk. The radial stress at the rigid inclusion-annular disk interface increases sharply and is much larger than the circumferential stress, as depicted in Figure 13. Taking $k = 0.8$, the effect of thickness reduction parameter n on the radial and circumferential stress components is shown in Figure 14. The dimensionless angular velocity $\Omega_e = 1.3677$ is used, which corresponds to the elastic limit angular velocity for a uniform thickness disk. The magnitudes of stresses decrease with the reduction in disk thickness at the edge. The effect of the geometric parameter k on the variation of the elastic limit angular velocity with the thickness reduction at the edge is given in Figure 15. As n increases the elastic limit angular velocity for $k = 0.52$ increases sharply. The dependence of the elastic limit angular velocity on the parameter n

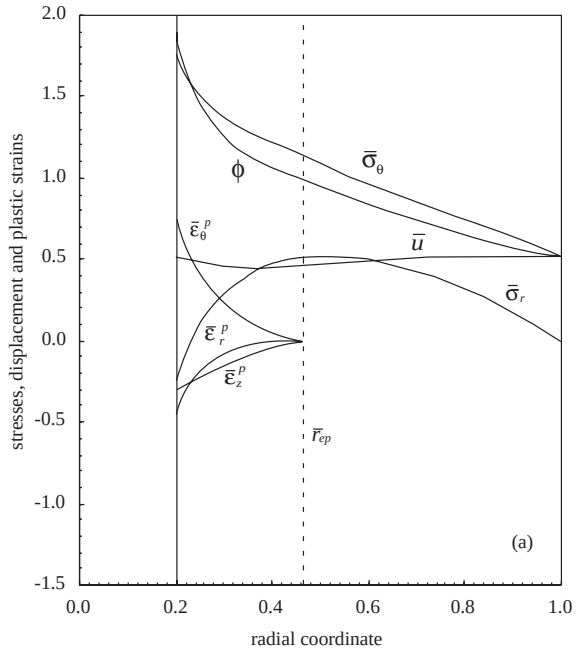

Figure 6. Elastic-plastic stresses, displacement and plastic strains for $n = 0.4$, $k = 2.4$, $H = 0.5$, $\bar{p} = 0.25$, $\Omega = 1.6$ (a) $m = 0.5$, (b) $m = 1$, (c) $m = 2$.

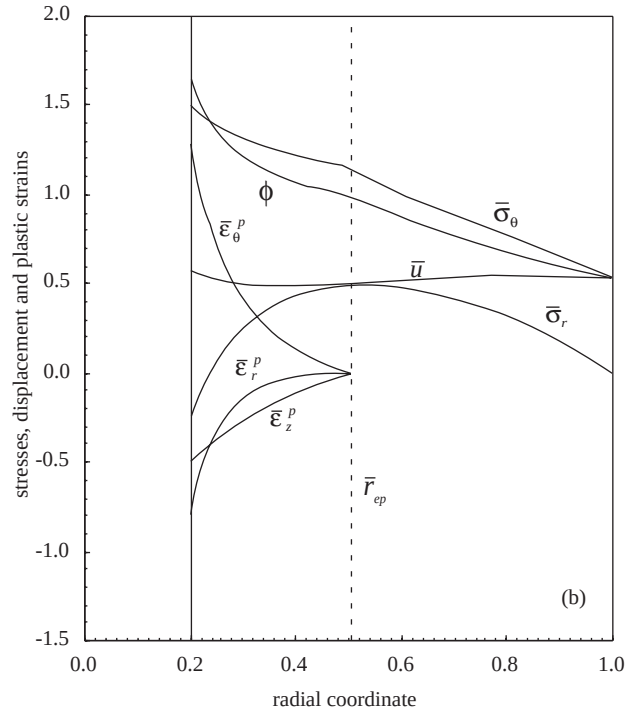

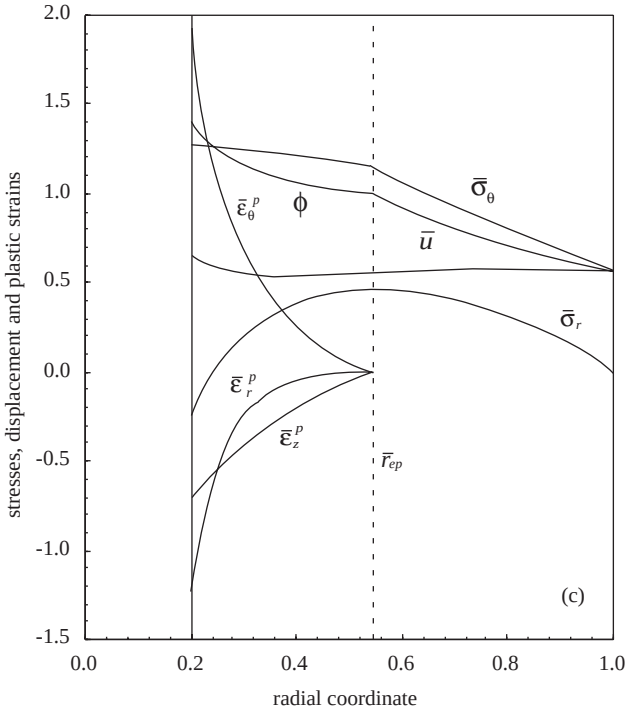

Figure 6. Contunied

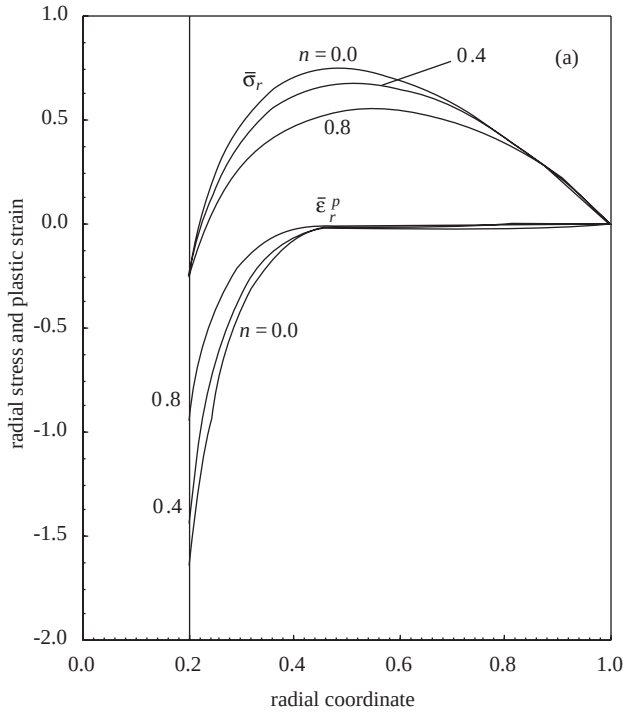

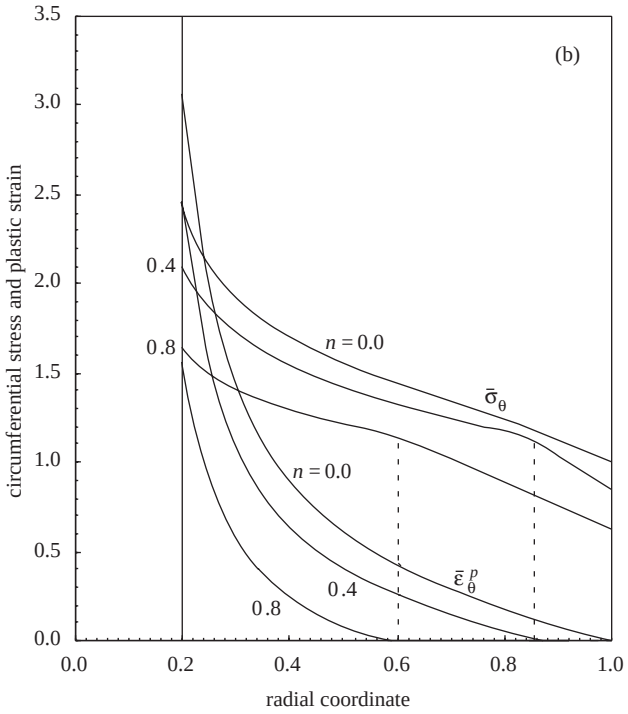

Figure 7. Elastic-plastic (a) radial stresses and plastic strains (b) circumferential stresses and plastic strains for $k = 1$, $H = 0.5$, $m = 1$, $\bar{p} = 0.25$ and $\Omega = 1.8635$ using n as a parameter.

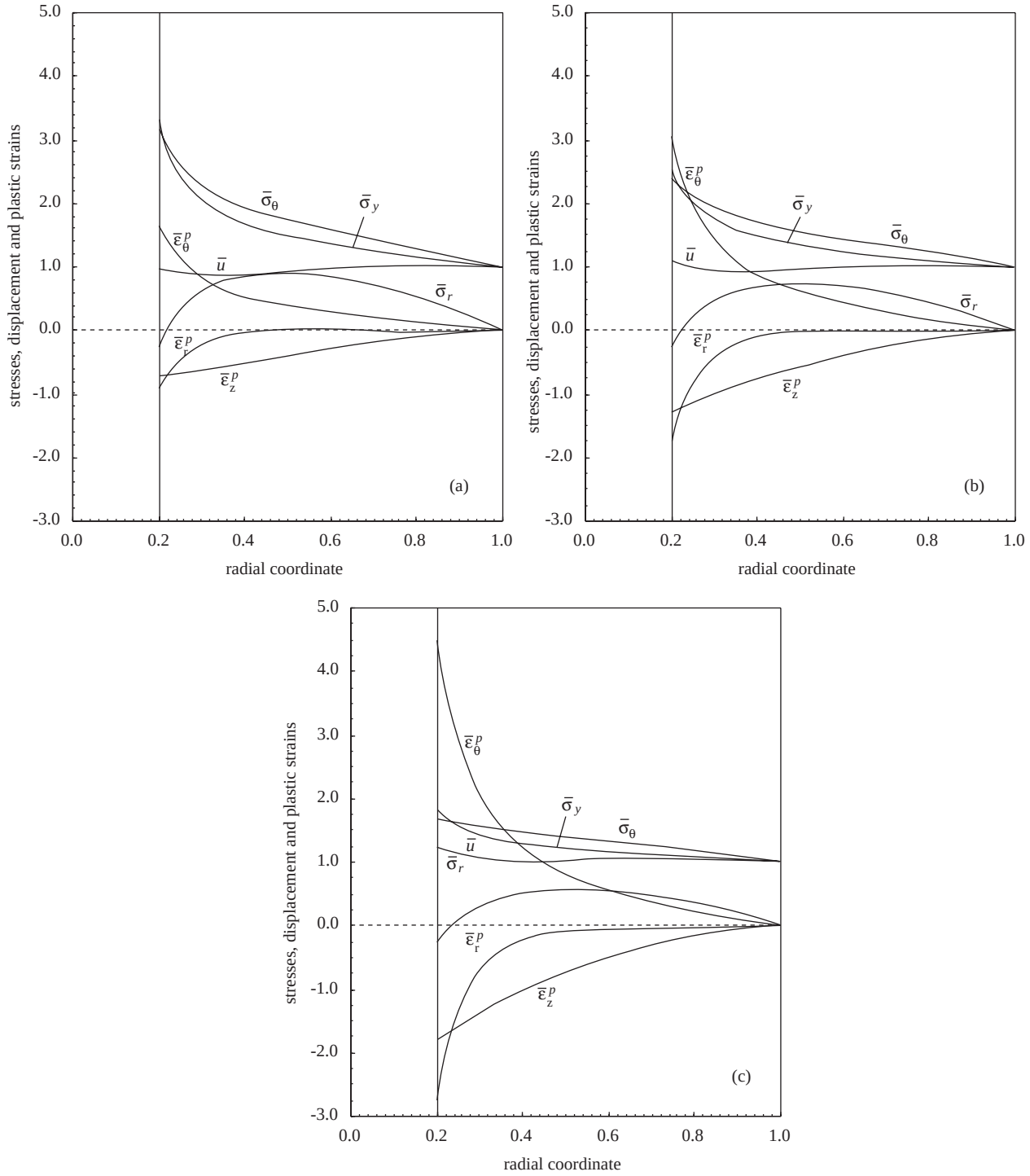

Figure 8. Fully plastic stresses, displacement and plastic strains for $n = 0.4$, $k = 2.4$, $H = 0.5$, $\bar{p} = 0.25$, (a) $m = 0.5$, $\Omega_{fp} = 2.1018$, (b) $m = 1$, $\Omega_{fp} = 1.9720$, (c) $m = 2$, $\Omega_{fp} = 1.8422$.

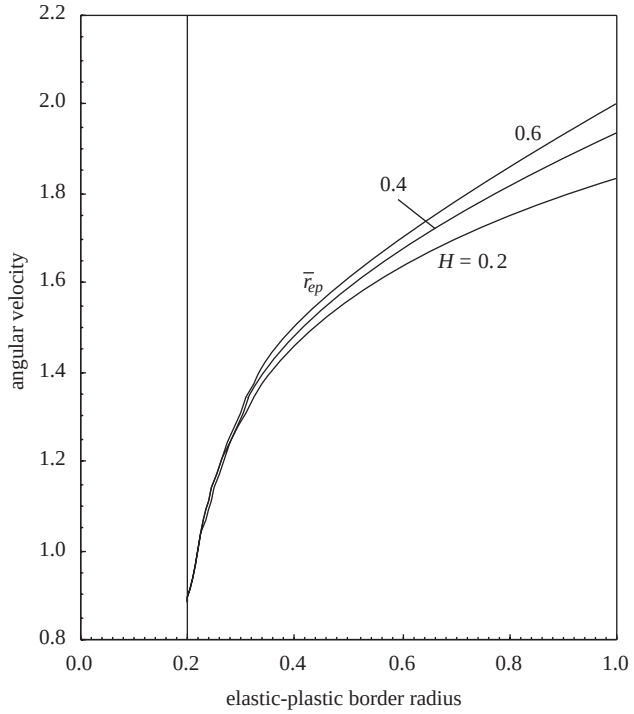

Figure 9. Propagation of elastic-plastic border radius for $n = 0.4$, $k = 2.4$, $\bar{p} = 0.25$, $m = 1$ using H as a parameter.

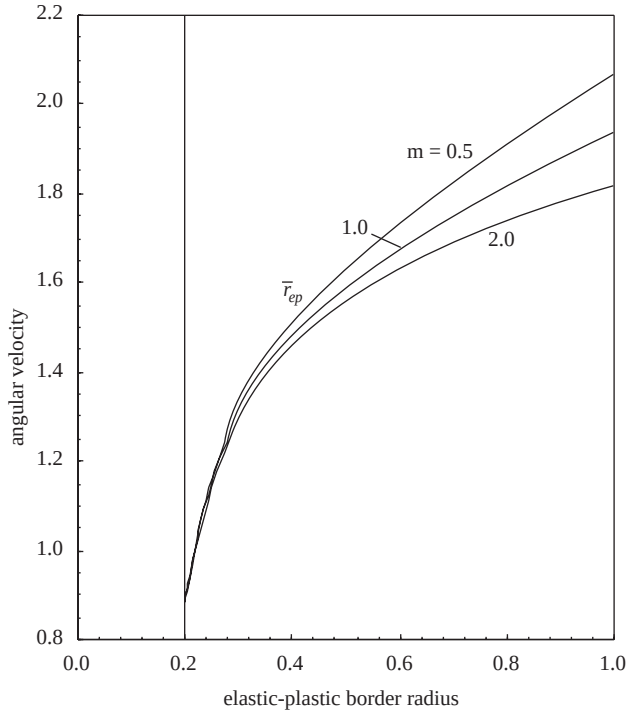

Figure 10. Propagation of elastic-plastic border radius for $n = 0.4$, $k = 2.4$, $\bar{p} = 0.25$, $H = 0.4$ using m as a parameter.

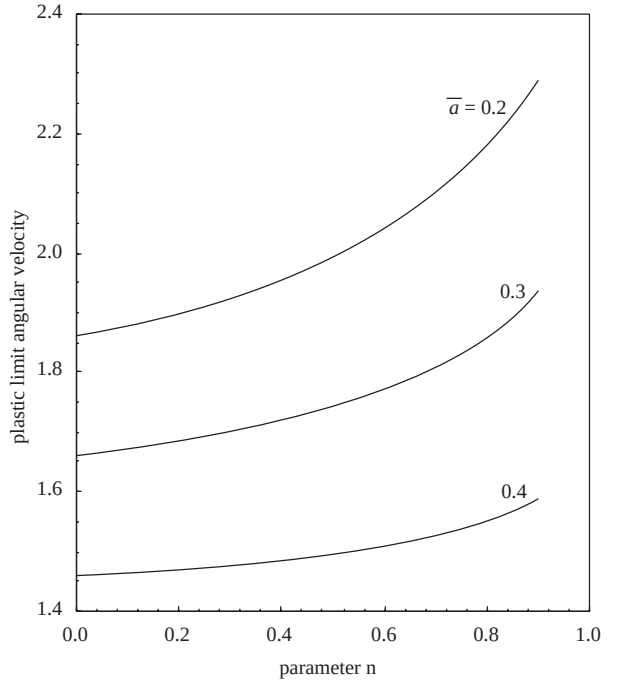

Figure 11. Variation of plastic limit angular velocity with the thickness reduction parameter n for different bore radii ($k = 1.0$, $H = 0.5$, $m = 1$, $\bar{p} = 0.25$).

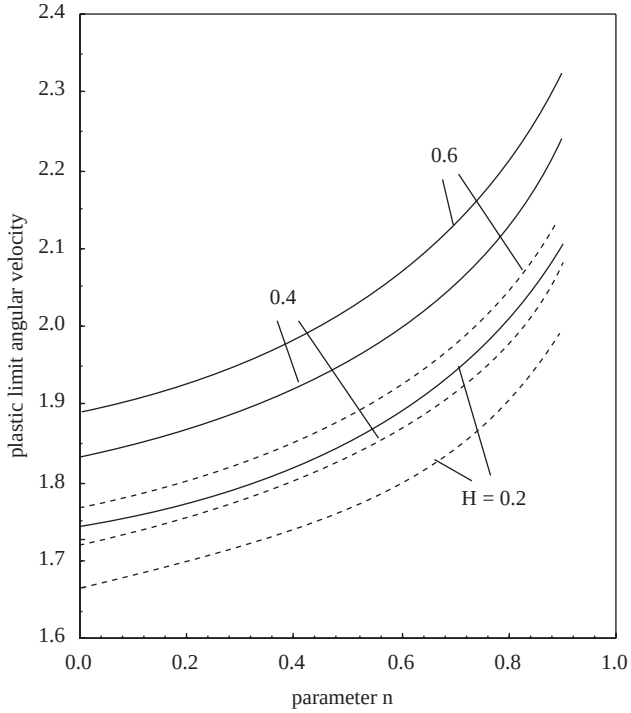

Figure 12. Variation of plastic limit angular velocity with the thickness reduction parameter n for $\bar{a} = 0.25$, $\bar{p} = 0.25$ using H and m as parameters (solid lines: $m = 1$, dashed lines: $m = 2$).

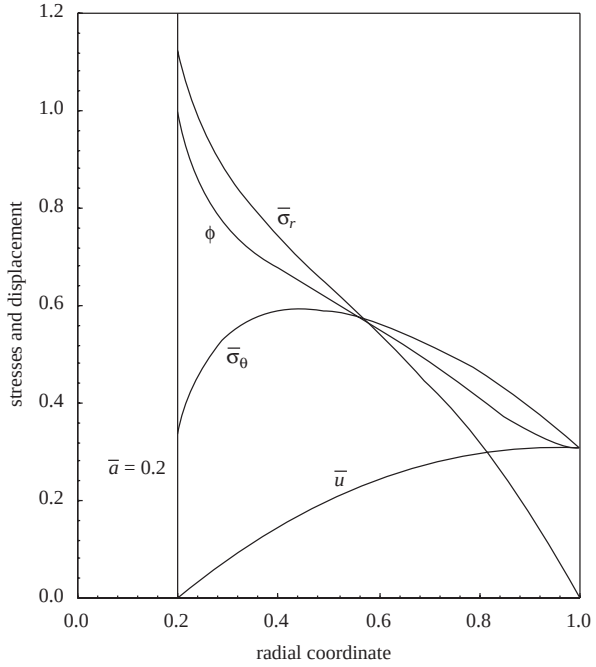

Figure 13. Stresses and displacement in a rotating annular disk with rigid inclusion for $\bar{a} = 0.2$, $n = 0.4$ and $k = 2.4$ at the elastic limit angular velocity $\Omega_e = 1.4925$.

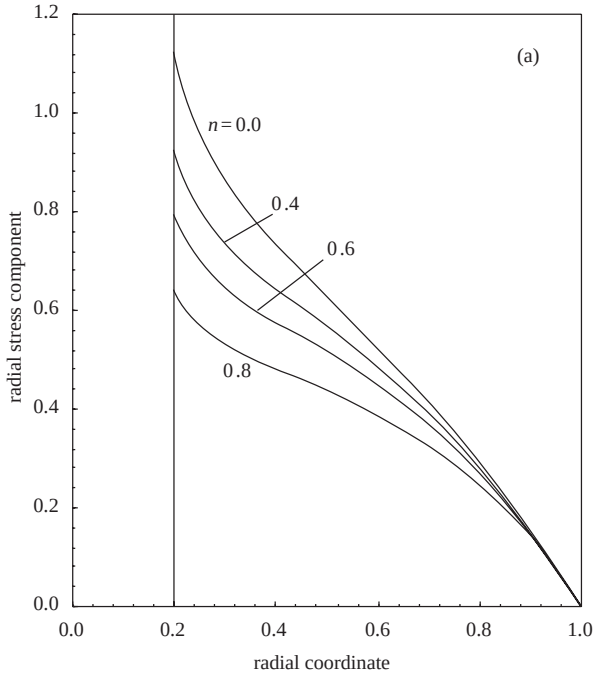

Figure 14. Comparison of (a) radial, (b) circumferential stresses for $k = 0.8$, $\Omega = 1.3677$ using n as a parameter.

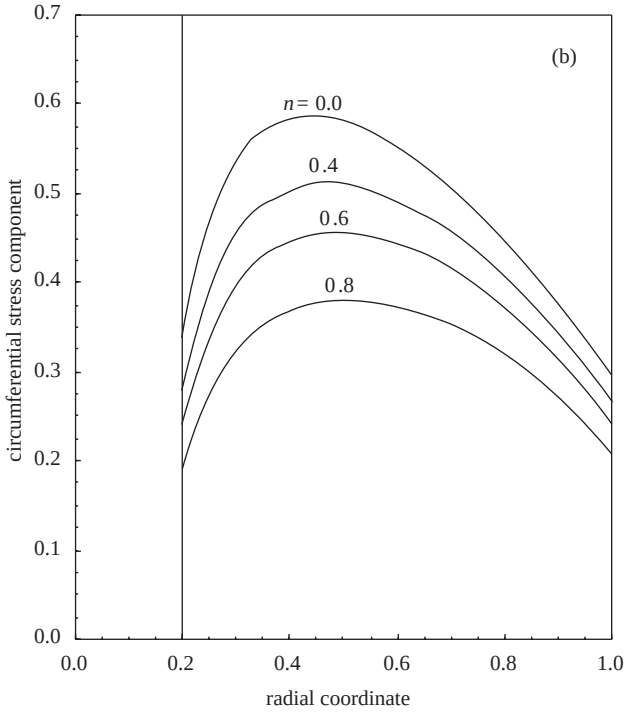

Figure 14. Contunied

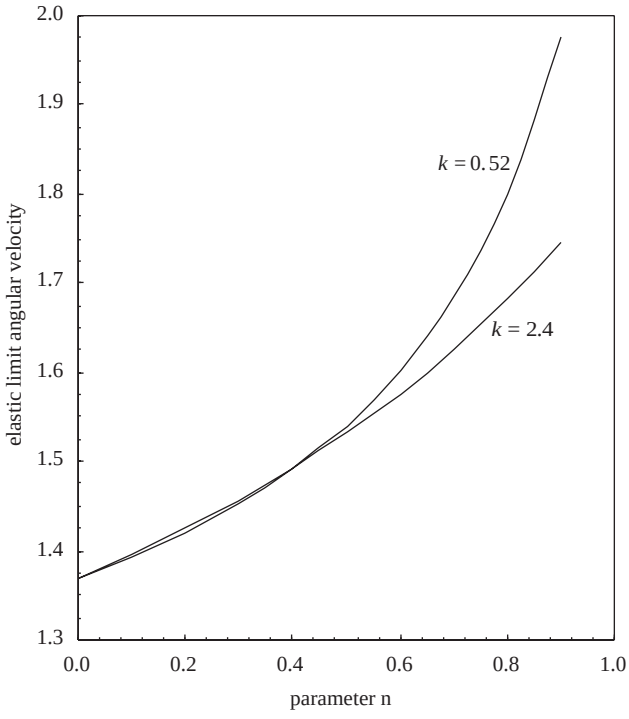

Figure 15. Variation of elastic limit angular velocity with the thickness reduction parameter n for $k = 0.52$ and $k = 2.4$.

for $\bar{a} = 0.1$, 0.2 and 0.3 is shown in Figure 16. As the radius of the rigid inclusion (or inner radius of the annular disk) decreases the elastic limit angular velocity increases. It is noted that the largest elastic limit angular velocity corresponds to the largest n and the smallest inclusion radius. The effect of the material parameter m, which represents the characteristics of the hardening rule, is investigated for a partially plastic disk using $m = 0.5$, 1 and 2 and the results are presented in Figure 17. It is found that although the stresses are almost the same the propagation of the plastic zone as well as the magnitudes of the plastic strains increase with increasing m values.

For $H = 0.5$ and $m = 1$ the fully plastic angular velocity of a uniform thickness disk is calculated as $\Omega_{fp} = 2.1743$. At this angular velocity the disk is partially plastic for larger n values. Taking $k = 1$, the elastic-plastic stresses for different n values together with the corresponding plastic strain components are plotted in Figure 18. The elastic-plastic border radius in each case is marked by the location where the plastic strains vanish. The stresses, plastic strains and the width of the plastic zone are all minimum for the largest value of n.

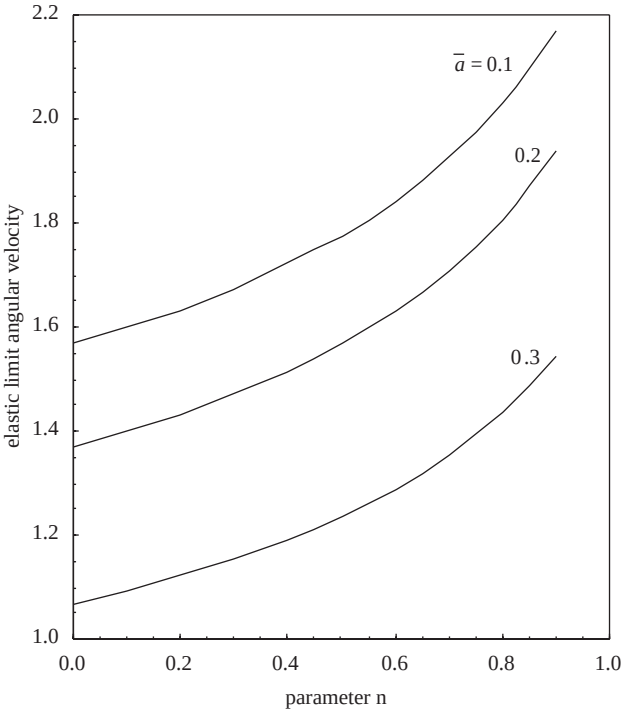

Figure 16. Variation of elastic limit angular velocity with the thickness reduction parameter n for different inclusion radii.

Figure 19 shows the stresses, radial displacement and plastic strains at the fully plastic state for $m = 0.5$, 1 and 2. The corresponding plastic limit angular velocities are $\Omega = 2.4688$, 2.3283 and 2.1865, respectively. Note that with increasing m the magnitudes of the stresses are lowered, whereas plastic strains become significantly larger.

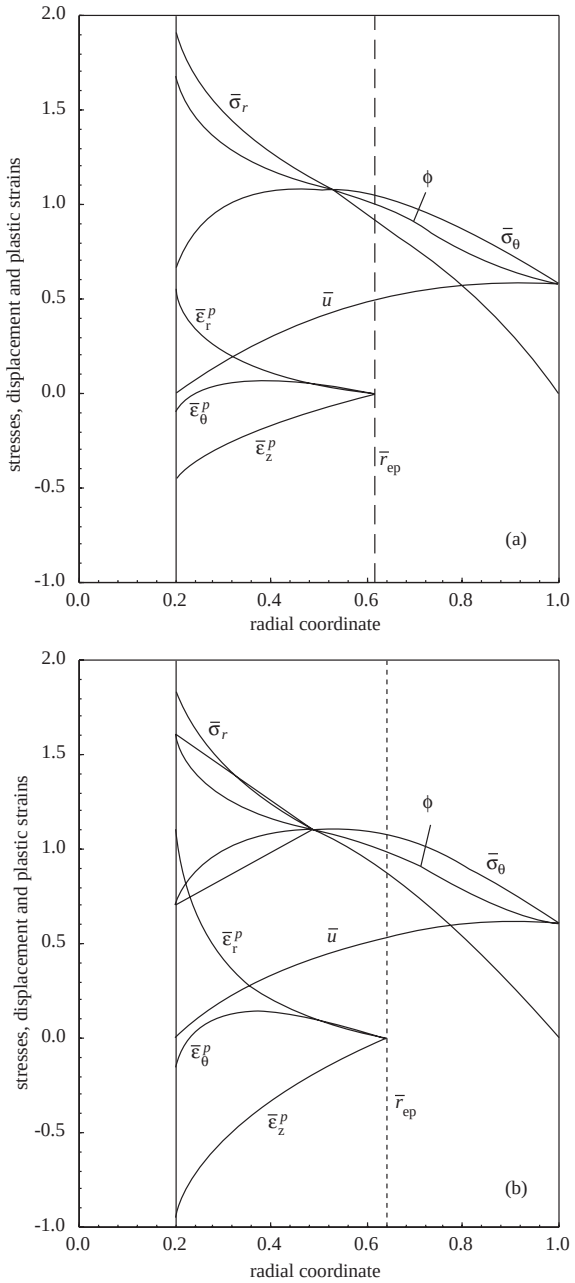

Figure 17. Elastic-plastic stresses, displacement and plastic strains for $n = 0.4$, $k = 2.4$, $H = 0.5$, $\Omega = 2.0$ (a) $m = 0.5$, (b) $m = 1$, (c) $m = 2$.

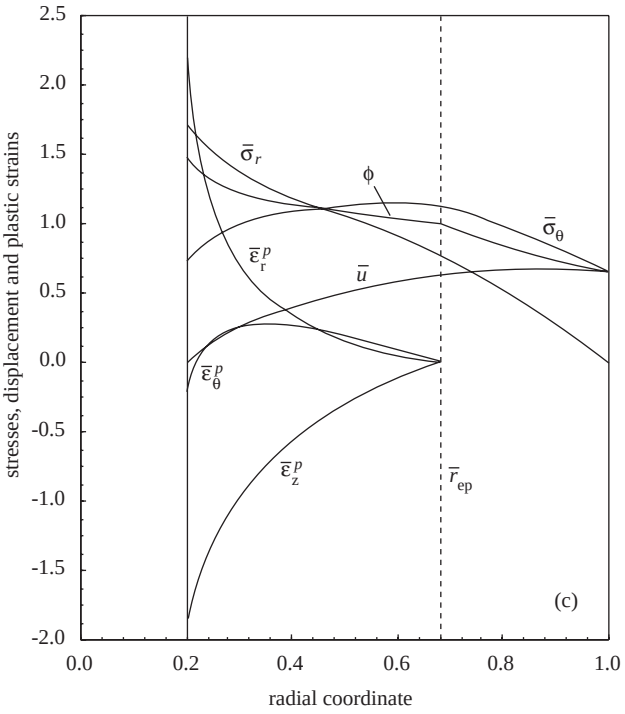

Figure 17. Contunied

The expansion of the elastic-plastic border radius $\bar{r}_{ep}$ with increasing angular velocity is calculated and displayed in Figures 20 and 21 for different values of the material and hardening parameters m and H, respectively. As expected, due to larger yield stress values corresponding to larger H and/or smaller m values (for a certain value of effective plastic strain) the propagation of the elastic-plastic border radius occurs at higher angular velocities. It is interesting to note that in the early stages of elastic-plastic deformation the propagation of r_{ep} occurs at a lower rate and is less sensitive to the hardening parameter H (and m) compared with the final stages of elastic-plastic deformation where the effect of H (and m) becomes significant. The plastic limit angular velocities for $H = 0.4$, $m = 0.5$, 1 and 2 are determined as $\Omega = 2.4321$, 2.2893 and 2.1566, respectively, and for $m = 1$, $H = 0.2$, 0.4 and 0.6 as $\Omega = 2.1769$, 2.2893 and 2.3604, respectively.

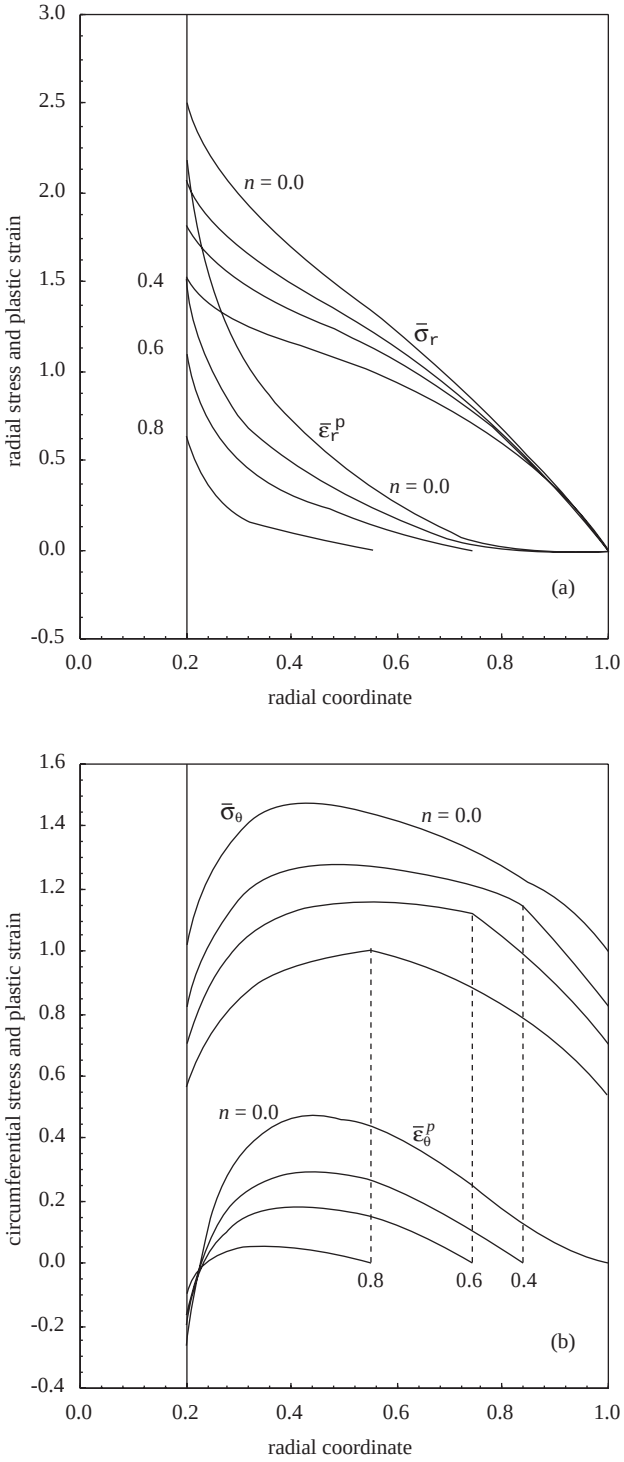

Figure 18. Elastic-plastic (a) radial stresses and plastic strains (b) circumferential stresses and plastic strains for $k = 1$, $H = 0.5$, $m = 1$, and $\Omega = 2.1743$ using n as a parameter.

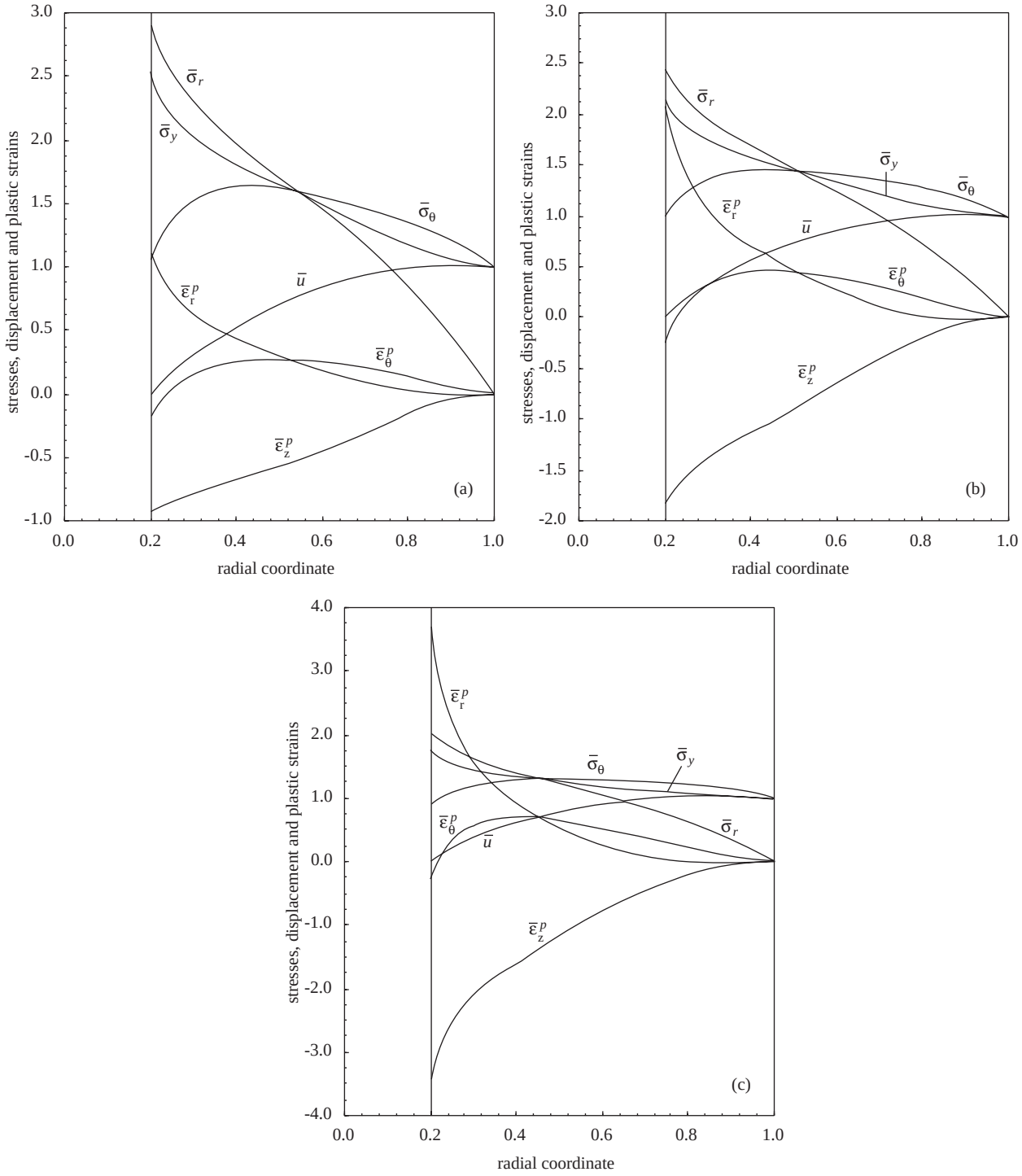

Figure 19. Fully plastic stresses, displacement and plastic strains for $n = 0.4$, $k = 2.4$, $H = 0.5$, (a) $m = 0.5$, $\Omega_{fp} = 2.4688$, (b) $m = 1$, $\Omega_{fp} = 2.3283$, (c) $m = 2$, $\Omega_{fp} = 2.1865$.

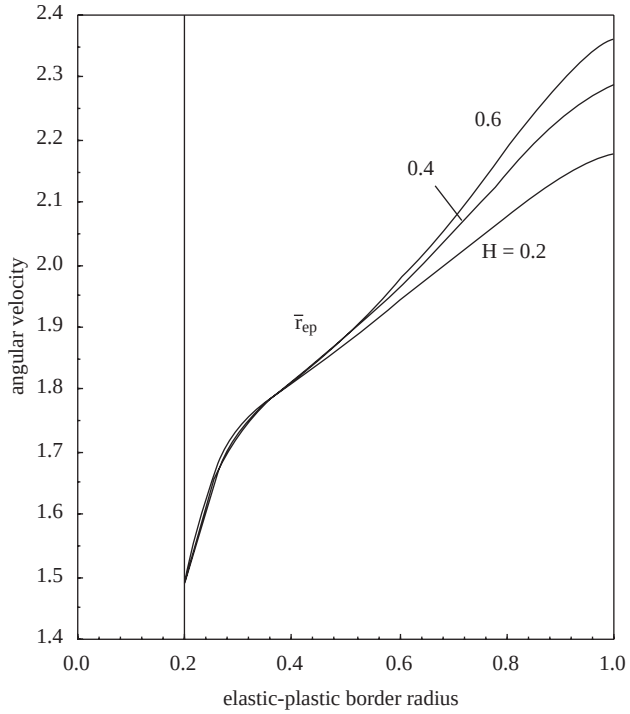

Figure 20. Propagation of elastic-plastic border radius for $n = 0.4$, $k = 2.4$, $m = 1$ using H as a parameter.

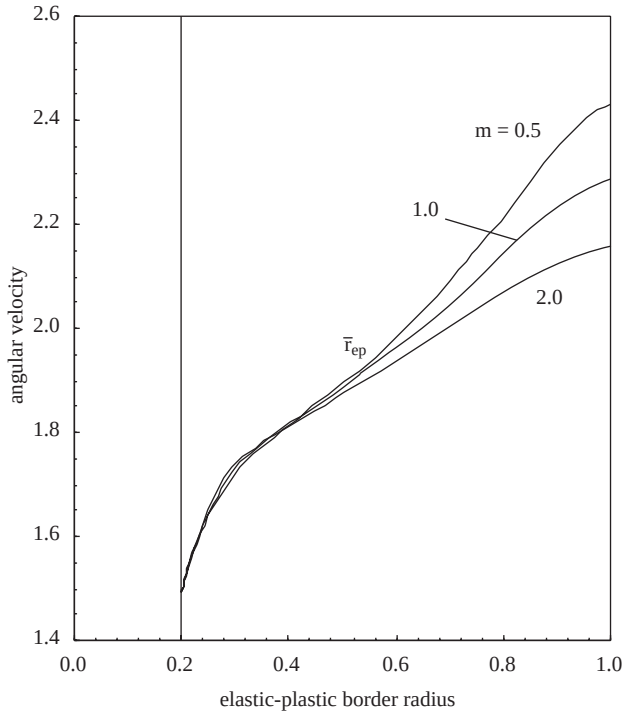

Figure 21. Propagation of elastic-plastic border radius for $n = 0.4$, $k = 2.4$, $H = 0.4$ using m as a parameter.

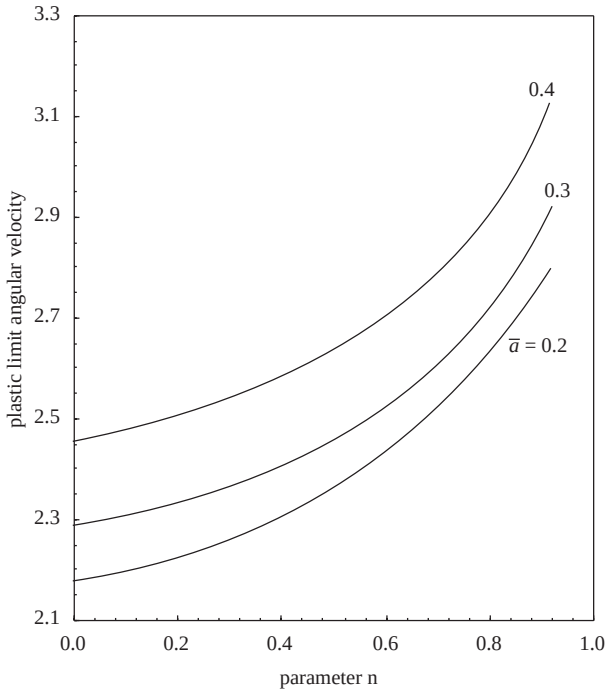

Figure 22. Variation of plastic limit angular velocity with the thickness reduction parameter n for different bore radii ($k = 1.0$, $H = 0.5$, $m = 1$).

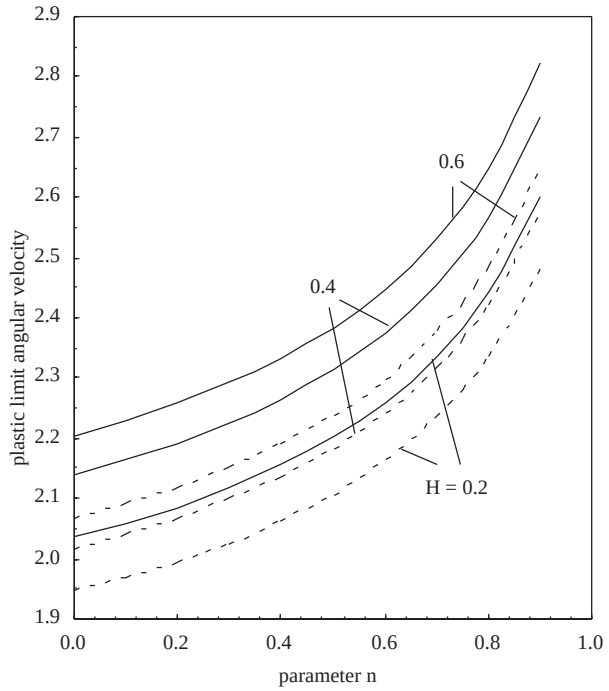

Figure 23. Variation of plastic limit angular velocity with the thickness reduction parameter n for $\bar{a} = 0.2$ using H and m as parameters (solid lines: $m = 1$, dashed lines: $m = 2$).

Figure 22 shows that for a certain thickness parameter n higher plastic limit angular velocities are encountered as the rigid inclusion radius a is increased. Finally, it is depicted in Figure 23 that the plastic limit angular velocity increases with increasing values of the parameter n for fixed values of the hardening parameters H and m. The fact that larger H and smaller m values lead to higher plastic limit angular velocities is also evident from this figure.

Concluding Remarks

Using an efficient numerical solution procedure, this article presents a von Mises solution to elastic-plastic stress distribution within rotating variable thickness annular disks with inner boundaries subjected to pressure or mounted on rigid inclusion. Non-linear isotropic strain hardening in the form of Swift's hardening law is considered. A comprehensive parametric analysis for elastic limit angular velocities, partially plastic behavior and plastic limit angular velocities is carried out to demonstrate the influence of all the geometric, material and hardening parameters involved. In particular, the dependence of the expansion of the plastic core on the thickness reduction parameters k and n together with the material parameters H and m governing the non-linear hardening behavior is investigated. Extensive numerical results pertaining to the parametric analysis are presented. These results indicate that in most cases the stresses, displacements and plastic strains, elastic and plastic limit angular velocities and width of the plastic region are affected significantly by the parameters used in the model.

References

Budiansky, B., "A Reassessment of Deformation Theories of Plasticity". ASME J. Appl. Mech. 26, 259-264, 1959.

Chakrabarty, J., Theory of Plasticity, McGraw-Hill, New York, 1987.

Chen, P.C.T., "A Comparison of Flow and Deformation Theories in a Radially Stressed Annular Plate". ASME J. Appl. Mech. 40, 283-287, 1973.

Chen, W.F. and Han, D.J., Plasticity for Structural Engineers. Springer, New York, 1988.

Eraslan, A.N., "Von Mises Yield Criterion and Nonlinearly Hardening Variable Thickness Rotating Annular Disks with Rigid Inclusion". Mech. Res. Comm. 29, 339-350, 2002.

Eraslan, A.N. and Argeso, H., "Limit Angular Velocities of Variable Thickness Rotating Disks". Int. J. Solids Struct. 39, 3109-3130, 2002.

Eraslan, A.N. and Orçan, Y., "Elastic-Plastic Deformation of a Rotating Solid Disk of Exponentially Varying Thickness". Mech. Mat. 34, 423-432, 2002a.

Eraslan, A.N. and Orçan, Y., "On the Rotating Elastic-Plastic Solid Disks of Variable Thickness Having Concave Profiles". Int. J. Mech. Sci. 44, 1445-1466, 2002b.

Gamer, U., Elastic-Plastic Deformation of the Rotating Solid Disk". Ingenieur-Archiv. 54, 345-354, 1984.

Güven, U., Elastic-Plastic Stresses in a Rotating Annular Disk of Variable Thickness and Variable Density". Int. J. Mech. Sci. 34, 133-138, 1992.

Güven, U., "The Fully Plastic Rotating Disk with Rigid Inclusion". ZAMM., 77, 714-716, 1997.

Güven, U., "Elastic-Plastic Stress Distribution in Rotating Hyperbolic Disk with Rigid Inclusion". Int. J. Mech. Sci. 40, 97-109, 1998.

Hindmarsh, A.C., "ODEPACK: A Systematized Collection of ODE Solvers". In: Scientific Computing, (Stepleman, R.S., Ed.), North Holland, Amsterdam, 1983.

Jahed, H., Lambert, S.B. and Dubey, R.N. "Total Deformation Theory for Non-Proportional Loading". Int. J. Press. Vessels and Piping 75, 633-642, 1998.

Ma, G., Hao, H. and Miyamoto, Y., "Limit Angular Velocity of Rotating Disc with Unified Yield Criterion". Int. J. Mech. Sci. 43, 1137-1153, 2001.

Yeh, K.Y. and Han, R.P.S., "Analysis of High-Speed Rotating Disks with Variable Thickness and Inhomogeneity". J. Appl. Mech., Trans. ASME., 61, 186-191, 1994.

You, L.H., Long, S.Y. and Zang, T.J., "Perturbation Solution of Rotating Solid Disks with Nonlinear Strain Hardening". Mech. Res. Comm. 24, 649-658, 1997.

You L.H., Tang Y.Y., Zhang, J.J. and Zheng, C.Y., "Numerical Analysis of Elastic-Plastic Rotating Disks with Arbitrary Variable Thickness and Density". Int. J. Solids Struct. 37, 7809-7820, 2000.

You, L.H. and Zhang, J.J., "Elastic-Plastic Stresses in a Rotating Solid Disk". Int. J. Mech. Sci. 41, 269-282, 1999.